Chinese Journal of Structural Chemistry

ARTICLE

Ingenious Design of CoAl-LDH p-n Heterojunction Based on CuI as Holes Receptor for Photocatalytic Hydrogen Evolution

Yue Cao[1], Hongqian Gou[1], Pengfei Zhu[2] and Zhiliang Jin[1]*

[1]*School of Chemistry and Chemical Engineering, Key Laboratory for Chemical Engineering and Technology, State Ethnic Affairs Commission, Ningxia Key Laboratory of Solar Chemical Conversion Technology, North Minzu University, Yinchuan 750021, China*

[2]*School of Environmental Science and Engineering, Shaanxi University of Science and Technology, Xi'an 710021, China*

ABSTRACT Reasonable design of heterojunction can greatly improve the photocatalytic hydrogen evolution activity of materials. Herein, p-n heterojunction of 2D/3D structure is constructed by the nanosheet of CoAl-LDH and rock-like CuI. The introduction of CuI can make CoAl-LDH disperse better, which brings more reaction sites for the hydrogen evolution reaction. Meanwhile, the 2D/3D structure is conducive to the construction of p-n heterojunction between the CoAl-LDH and CuI. The optical and electrochemical properties of the material indicate that the separation and transference of photon-generated carriers are promoted by the p-n heterojunction. The activity of composite catalyst (CI-10) reaches a maximum of 3.59 mmol g^{-1} h^{-1} which is 28.5 times higher than that of CuI. Furthermore, the influence of the amount of CuI and pH value on the hydrogen evolution reaction is explored. Based on the band structures of CoAl-LDH and CuI, the mechanism of photocatalytic reaction of CI-10 is proposed. The p-n heterojunction constructed with the CuI as hole receptor provides a new way to enhance the activity of photocatalytic H_2 evolution.

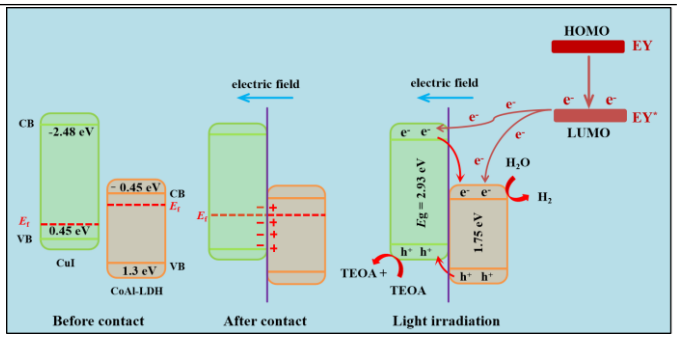

Keywords: CoAl-LDH, CuI, p-n heterojunction, photocatalysis, hydrogen production

INTRODUCTION

As is known to all, the traditional fossil energy is non-renewable resources[1,2]. In recent years, the forward rise of economy leads to the vast depletion of fossil energy. However, the fossil energy is still used as the main energy. Hence, the vigorous development and effective utilization of clean energy are very important and meaningful. Solar energy, a promising alternative to fossil fuels, has been extensively studied[3-5]. Converting it into hydrogen is a crucial way to efficiently use light energy[6,7]. In order to achieve this process, scientists have developed a number of photocatalysts, such as, CdS[8,9], g-C_3N_4[10-12], ZnInS[13,14] and TiO_2[15,16]. But, there are many issues to overcome in a single semiconductor including fast recombination of photon-generated carriers, insufficient surface reactive sites, and low reducing power[17,18]. Therefore, scientists have proposed ways to build heterojunctions to overcome these problems[19-21]. Generally, the heterojunction includes p-n heterojunction, Z-scheme, and S-scheme.

It is reported that the construction of heterojunction is based on two semiconductors having suitable band structure. For example, Liu's group reported that the CoAl-LDH/BiOBr heterojunction was used for the degradation of pollutant[22]. The photocatalytic degradation performance of the heterojunction achieved enhancement because the CoAl-LDH and BiOBr showed nanosheets structure and formed the two-dimensional (2D/2D) Z-scheme heterojunction. In addition, Xia's group reported a novel three-dimensional (3D) Z-scheme heterojunction of the Bi_2O_3@CoAl-LDHs[23]. This heterojunction showed excellent performance of photocatalytic ammonia synthesis because it significantly improved the lifetime of photon-generated carriers and the transference efficiency of electrons. Li et al. reported that $Zn_xCd_{1-x}S$ is dispersed on the CoAl-LDH to form heterojunctions[24]. This heterojunction revealed favourable activity of photocatalytic hydrogen evolution. Obviously, semiconductors with appropriate band gaps can better construct heterojunctions.

The CoAl-LDH is 2D layered materials composed of Co^{2+} and Al^{3+} metal cations coordinated to hydroxide ions, and are charge-balanced by intercalated CO_3^{2-}[25]. Metal cations are located at the centers of edge sharing octahedra, and its vertexes are connected with OH-, which forms extended two-dimensional nanosheets[26]. The CoAl-LDH not only has an appropriate band structure but also shows a nanosheet structure, which can be beneficial to the formation of heterojunction and combine with materials of different dimensions to form a unique structure. Moreover, the p-type CuI has an advantage of high hole mobility in the construction of heterojunction. For instance, Sun's group reported that the BiOI/CuI heterojunction is constructed by using the CuI as hole transport channel[27]. The BiOI/CuI composite shows excellent photoelectrocatalytic performances, which confirms that the p-type CuI is ideal hole transport channel for enhancing traditional semiconductor H_2 evolution activity. Zhang's team reasonably designed CuI-GD/g-C_3N_4 composite material[28]. Based on the unique advantages of CoAl-LDH and CuI, a 2D/3D p-n heterojunction was constructed.

In this work, a 2D/3D p-n heterojunction was synthesized by a simple hybrid method for photocatalytic hydrogen production. The role of internal electric field in p-n heterojunction and effective dispersion of CoAl-LDH on CuI render high hydrogen evolution acti-

DOI: 10.14102/j.cnki.0254-5861.2022-0042

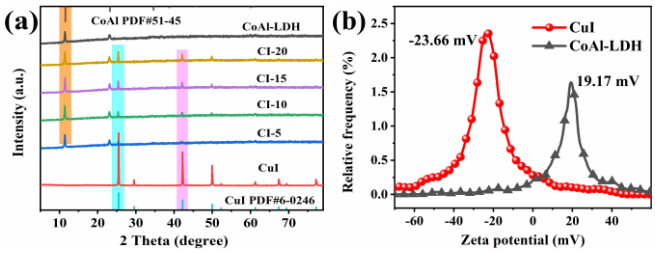

Figure 1. (a) XRD patterns of all catalysts; (b) Zeta potential of CoAl-LDH and CuI.

vity of 3.59 mmol g^{-1} h^{-1}. Furthermore, the band structures of CoAl-LDH and CuI were further explored by the UV-vis diffuse reflectance spectra (DRS) and X-ray photoelectron spectroscopy (XPS) valence band spectra and the photocatalytic mechanism of p-n heterojunction for hydrogen production was proposed.

■ RESULTS AND DISCUSSION

XRD and Zeta Potential Discussion. The XRD patterns of all catalysts are shown in Figure 1a to reveal crystal structures of catalysts. Peaks of CoAl-LDH are consistent with that of the standard cards (PDF#51-45). The peaks located at 2θ = 11.4° and 23.1°, corresponding to two lattice planes (003, 006) of the CoAl-LDH, respectively. Similarly, the diffraction peaks of CuI identify with that of the cards (PDF#6-0246). The CuI has three distinct characteristic peaks (2θ = 25.4°, 42.2°, 49.9°). They are distributed to three lattice planes (111, 220, 311) of the CuI. Remarkably, both diffraction peaks of CoAl-LDH and CuI appear in the composite catalyst. XRD patterns of all catalysts confirm that they have been successfully synthesized. Moreover, the electronegativity of CoAl-LDH and CuI is revealed in Figure 1b. The zeta potentials of 19.17 and -23.66 mV belong to CoAl-LDH and CuI, respectively. Obviously, their zeta potential is opposite, which is beneficial to the formation of heterojunctions between CoAl-LDH and CuI because of the Coulomb electrostatic interaction between them[29].

SEM Analysis. The surface morphology of catalysts is explored by the SEM in Figure 2. Clearly, the surface morphology of CoAl-LDH is nanosheet in Figure 2a. However, the morphology of CuI is similar to rock in Figure 2b, which is quite different from that of CoAl-LDH. In Figure 2c, both the nanosheets of CoAl-LDH and rock-like CuI are observed, which indicates that composite catalyst has been successfully synthesized. On the side, the 2D/3D structure is clearly revealed and the CoAl-LDH is well dispersed on CuI, which is conducive to the construction of p-n heterojunction between CoAl-LDH and CuI and promotes the photocatalytic hydrogen evolution performance of CI-10. To further confirm the distribution of CoAl-LDH and CuI, elemental mapping is provided (Figure 2d), illustrating the distribution of Co, Al, O, Cu and I elements throughout the CI-10.

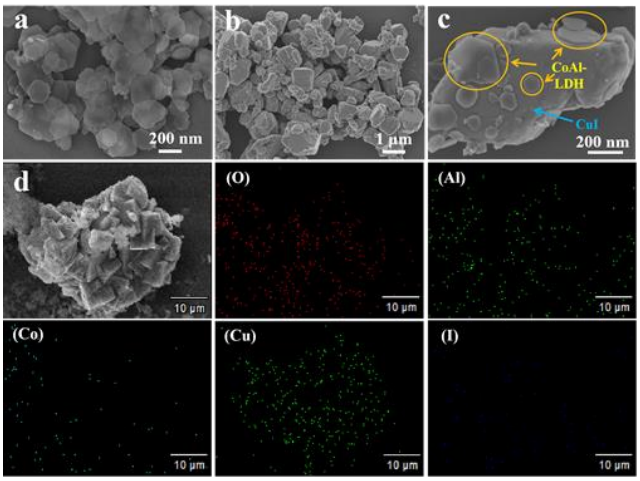

Figure 2. The SEM images of (a) CoAl-LDH and (b) CuI, and (c) CI-10; (d) Elemental mapping images of CI-10.

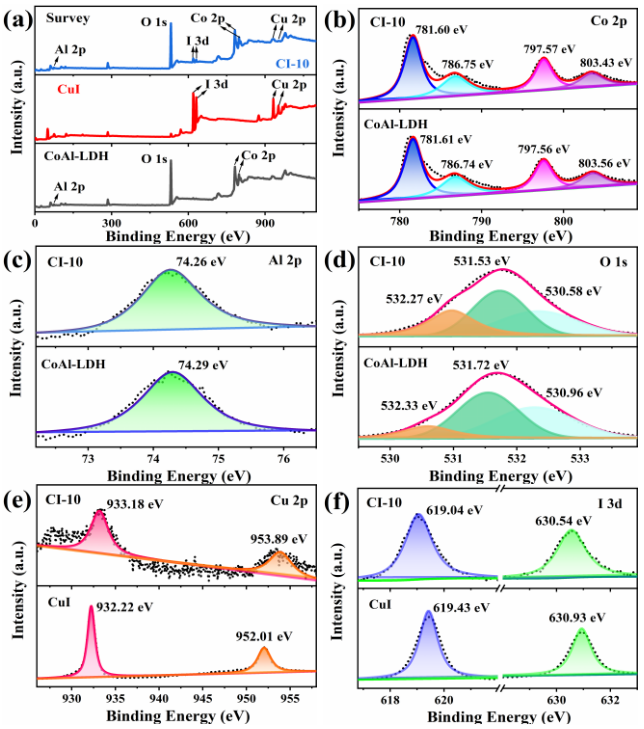

Figure 3. (a) Survey spectra of CoAl-LDH, CuI, and CI-10; High-resolution spectra of (b) Co, (c) Al, (d) O, (e) Cu, and (f) I.

XPS Discussion. The surface chemical compositions of CoAl-LDH, CuI, and CI-10 are explored by XPS, as shown in Figure 3. Their survey spectra are exhibited in Figure 3a. In order to eliminate test errors, we corrected all XPS testing data based on sp^2 C of adventitious carbon at 284.8 eV. The peaks belonging to Al, O, and Co elements are shown in the survey spectra of CoAl-LDH. Similarly, the peaks pertained to Cu and I appear in the spectra of CuI. Notably, the spectra of CI-10 contain characteristic peaks of all elements in CoAl-LDH and CuI. In Figure 3b, high-resolution XPS spectra in the CoAl-LDH, the peaks at 781.61 and 797.56 eV can be distributed to the typical Co $2p_{3/2}$ and $2p_{1/2}$ while the other peaks (786.74 and 803.56 eV) belong to high-spin divalent Co^{2+} atoms[30]. Moreover, the peak at 74.29 eV ascribes to Al^{3+} atoms in Figure 3c. The peaks at 532.27, 531.53, and 530.58 eV in O 1s spectra can be assigned to the chemisorbed water, oxygen atoms in the vicinity of an oxygen vacancy and hydroxyl, respectively[31-33].

Chin. J. Struct. Chem. **2022**, 41, 2206079-2206085
DOI: 10.14102/j.cnki.0254-5861.2022-0042

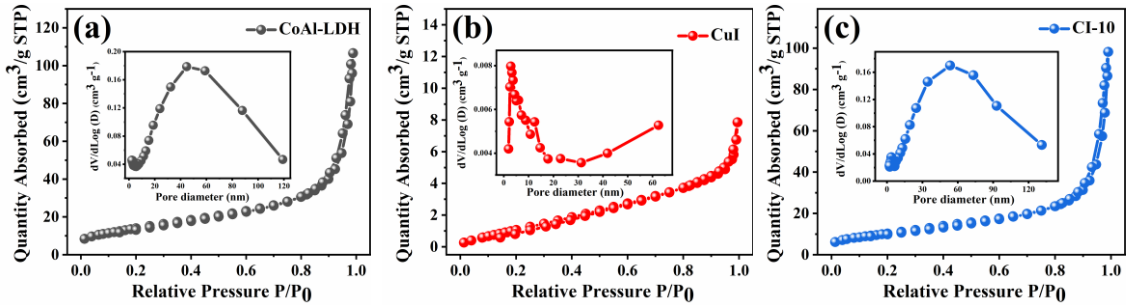

Figure 4. (a-c) The adsorption desorption isotherms and pore size curves (inset) of CoAl-LDH, CuI, and CI-10.

The two peaks belonging to Cu $2p_{1/2}$ and Cu $2p_{3/2}$ are located at 952.01 and 932.22 eV in Figure 3e, respectively, which is ascribed to the Cu^+ atoms[34]. In Figure 3f, the two peaks at 619.43 and 630.93 eV are assigned to I $3d_{5/2}$ and I $3d_{3/2}$[27]. Compared with CoAl-LDH and CuI, the binding energies of Co, Al and O elements in CI-10 change slightly, which indicates that the valence of these elements has not changed. But, the binding energy of Cu element in CI-10 increases, manifesting the existence of Cu^{2+}, which may be due to oxidation[35]. Meanwhile, the binding energy of I element in CI-10 is decreased.

BET Analysis. The specific surface areas (S_{BET}) of CoAl-LDH, CuI, and CI-10 are tested, as shown in Figure 4. Their adsorption isotherm is the Type-IV in Figure 4a[36]. Furthermore, as shown in the inset of Figure 4(b-d), their pore diameters mainly spread in the range of 0-25 nm. Hence, these catalysts are mesoporous materials. Table 1 shows their data of physical adsorption. The S_{BET} of CoAl-LDH, CuI, and CI-10 is 52, 6, and 38 $m^2\ g^{-1}$, respectively. Compared with the S_{BET} of CoAl-LDH, that of CI-10 decreases, which may be caused by the CuI's small S_{BET}. The CI-10 has little variation in pore volume and average pore diameter. Generally, the increase of S_{BET} and average pore diameter can promote photocatalytic H_2 evolution activity of the catalyst. Hence, the enhancement of photocatalytic performance of CI-10 has nothing to do with the variation of S_{BET} and average pore diameter and may have something to do with the p-n heterojunction.

Photocatalytic Activity. The photocatalytic H_2 evolution performance of all catalysts is evaluated by the EY sensitization. In Figure 5a, the pure CoAl-LDH and CuI have weak activity of 0.49 and 0.12 mmol g^{-1} h^{-1} after five hours of reaction, respectively, which may be due to the fast recombination of photon-generated carriers in a single semiconductor. When the two semiconductors are combined, the H_2 evolution activity of compound catalyst CI-5 is greatly improved to 2.56 mmol g^{-1} h^{-1} due to the p-n heterojunction. When the amount of CuI is increased, the performance of CI-10 reaches a maximum of 3.59 mmol g^{-1} h^{-1}. With increasing the amount of CuI, the activity of CI-15 significantly decreases, which may result from the abundance of rock-like CuI shielding the active sites of the reaction. Moreover, the experiment result shows that CI-10 has little activity in the absence of EY. Hence, EY is essential for the photocatalytic hydrogen evolution of CI-10. It reveals the effect of pH value on the H_2 evolution activity (Figure 5b). When pH = 9, CI-10 has the best H_2 evolution performance. However, lowering the pH to 8 leads to a decrease in the performance of CI-10, which is attributed to the protonation of TEOA, leading to its reduced role as an electron donor[37]. With increasing the pH, the performance of CI-10 decreases gradually because of the decreased concentration of H^+. Hence, the influence of pH on hydrogen production performance of catalyst should be taken into account seriously. In Figure 5b, the samples are recycled to evaluate the stability of the catalyst. The experimental result shows that the stability of CI-10 is inadequate, which may need further improvement. Furthermore, the apparent quantum efficiency (AQE) of CI-10 is shown in Figure 5d. Obviously, the AQE of CI-10 reaches the highest at 520 nm single wavelength because the maximum absorption wavelength of EY is observed at 518 nm.

Table 1. S_{BET} and Pore Structures of the Catalysts

Compounds	S_{BET} ($m^2\ g^{-1}$)	Pore volume ($cm^3\ g^{-1}$)	Average pore size (nm)
CoAl-LDH	52	0.16	14
CuI	6	0.01	7
CI-10	38	0.15	16

UV-vis DRS Discussion. The optical performance of CI-10, CoAl-LDH, and CuI is assessed via the UV-vis DRS. In Figure 6a, the absorbance curves of CoAl-LDH and CuI are the same as the

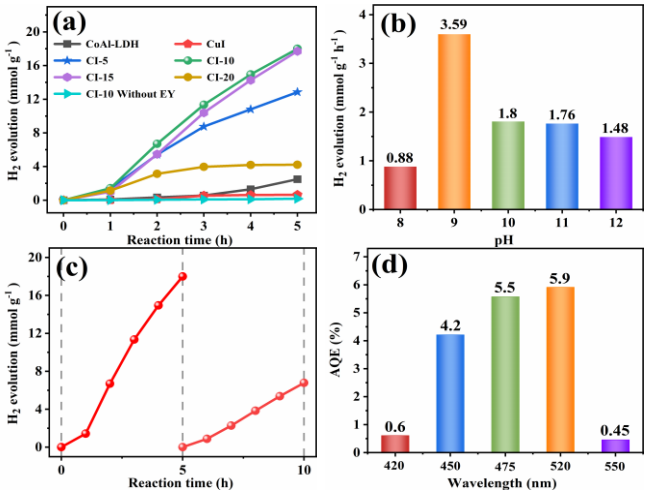

Figure 5. (a) The photocatalytic H_2 evolution activity of all catalysts; (b) The photocatalytic performance of CI-10 in different pH value; (c) The stability performance of CI-10; (d) The AQE of CI-10.

DOI: 10.14102/j.cnki.0254-5861.2022-0042

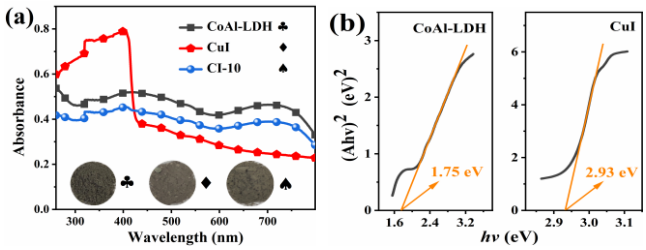

Figure 6. (a) The absorbance curves of CoAl-LDH, CuI, and CI-10; (b) Band-gap of CoAl-LDH and CuI.

previous reports[38,39]. The absorbance of CI-10 increases higher than that of CuI in the 420-800 nm range but lower than that of CoAl-LDH, which can be ascribed to the CuI's low absorbance. Although the CI-10 has a lower absorbance than CoAl-LDH, the absorbance is not decisive condition in the activity of photocatalytic hydrogen evolution. Therefore, the improvement of CI-10 photocatalytic activity should be related to p-n heterojunction between CoAl-LDH and CuI. Furthermore, the band-gap energies (E_g) of CoAl-LDH and CuI are obtained by equation (1). The E_g of CoAl-LDH and CuI is 1.75 and 2.93 eV, as shown in Figure 6b.

$$(ahv)^2 = A(hv - E_g) \qquad (1)$$

Where *a* is absorption coefficient, E_g the band-gap energy, *A* a constant, *h* a Planck constant, and v the frequency.

PL Spectra, TR-PL, LSV, and XPS Valence Band Spectra Discussion. The PL spectra of EY, CoAl-LDH, CuI, and CI-10 are revealed to evaluate the behaviors of photogenerated electrons

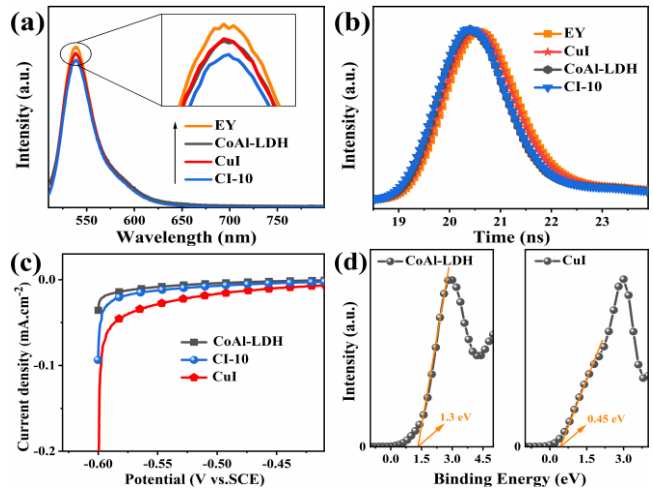

Figure 7. (a) The PL spectra of EY, CoAl-LDH, CuI, and CI-10; (b) The TRPL spectra of EY, CoAl-LDH, CuI, and CI-10; (c) LSV curves of CoAl-LDH, CuI, and CI-10; (d) The XPS valence band spectra of CoAl-LDH and CuI.

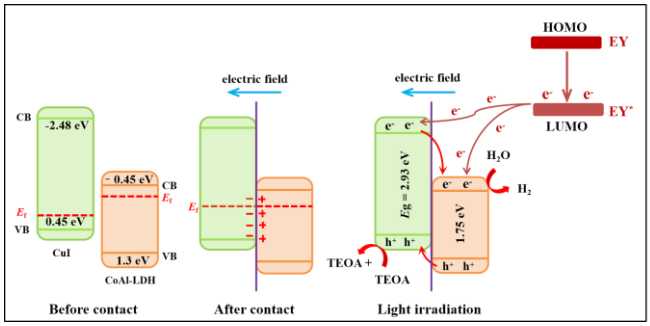

Figure 8. Photocatalytic hydrogen evolution mechanism of CI-10.

in Figure 7a. Their fluorescence emission peak appears at 538 nm. It is well known that when the EY is excited, the electrons of excited state are produced. They have a very short lifetime. If they do not transfer efficiently, the excited state electrons will fluoresce as a radiative transition and eventually quench. Therefore, the solution of EY exhibits the strongest fluorescence peak. Compared with the fluorescence intensity of EY, CoAl-LDH, and CuI, the CI-10 has the lowest fluorescence intensity, which indicates that the CI-10 can divert efficiently excited electrons of EY and increase the number of electrons participating in reduction reaction. Hence, the CI-10 has the best H_2 evolution performance. In Figure 7b, the TR-PL decay curves of CI-10 are shown. Table 2 shows the fitting values of decay curves data of samples. The fitting average lifetime of catalysts is less than that of EY (0.3 ns), which indicates that the catalysts are better able to transfer electrons from EY. The average lifetime of CI-10 is less than that of CuI, suggesting that nonradioactive decay channels are opened[40,41]. Hence, the recombination of photo-generated carriers is suppressed effectively. Moreover, the LSV curves of CoAl-LDH, CuI, and CI-10 are tested (Figure 7c). The CI-10 has lower over-potential than CoAl-LDH, which is beneficial to photocatalytic H_2 production reaction[42]. In Figure 7d, the valence band potential of CoAl-LDH and CuI is determined by the XPS valence band spectra. The VB of CoAl-LDH is determined to be 1.3 eV. The valence band potential (E_{VB}) of CuI is 0.45 eV versus the NHE[43]. According to $E_{VB} = E_{CB} + E_g$, the E_{CB} of CoAl-LDH is -0.45 eV and E_{CB} of CuI is -2.48 eV.

Reaction Mechanism. Based on the energy band of materials, the mechanism of photocatalytic reaction of CI-10 is proposed in Figure 8. The majority carriers of CoAl-LDH are electrons because it is n-type semiconductor, however, those of CuI are holes as it is p-type semiconductor. Owing to the difference in carrier concentration, when they are contacted, the electrons of CoAl-LDH diffuse spontaneously into CuI. The holes are left in CoAl-LDH. The process of diffusion stops when the Fermi levels of

Table 2. Fitting Decay Data for Samples

Samples	τ_1 [ns]	τ_2 [ns]	τ_3 [ns]	τ_{ave} [ns]	χ^2
EY	0.29 (95.30%)	5.23 (4.70%)	/	0.30	0.90
CoAl-LDH	0.09 (94.43%)	1.31 (3.84%)	6.06 (1.73%)	0.10	0.82
CuI	0.25 (93.53%)	1.56 (4.03%)	6.52 (2.45%)	0.27	0.90
CI-10	0.18 (94.94%)	1.68 (3.11%)	6.17 (1.95%)	0.19	0.91

Chin. J. Struct. Chem. **2022**, 41, 2206079-2206085
DOI: 10.14102/j.cnki.0254-5861.2022-0042

CoAl-LDH and CuI are the same. The internal electric field is constructed in interface of CoAl-LDH and CuI. It is difficult to be excited by visible light due to the wide band-gap of CuI[43]. Hence, CuI can act as hole receptor. Under the action of internal electric field, the holes in VB of CoAl-LDH are transferred to VB of CuI and expend finally by the TEOA. Electrons of CoAl-LDH take part in photocatalytic H_2 production reaction. The EY can produce electrons under visible light to supply the CoAl-LDH, and the reaction process has been previously reported[44]. The p-n heterojunction promotes greatly the separation of photon-generated carriers.

CONCLUSION

The synthesis of CoAl-LDH/CuI p-n heterojunction is successful. The 2D/3D structure formed by the nanosheet of CoAl-LDH and rock-like CuI brings more reaction sites for the photocatalytic reaction. Furthermore, the H_2 production experiment indicates that the photocatalytic activity of CI-10 is influenced by the amount of CuI and pH value. CI-10 has the strongest activity of photocatalytic hydrogen production due to the p-n heterojunction between the CoAl-LDH and CuI. The p-n heterojunction highly promotes the separation of photon-generated carriers under the effect of internal electric field. It has been confirmed that the CuI as a hole receptor can promote the transfer of holes. This paper contributes fresh method for improving the performance of photocatalytic H_2 evolution.

EXPERIMENTAL

Preparation of Composite. The CoAl-LDH was prepared from previous reports[44]. The CuI is a commercial one. Subsequently, 0.2 g CoAl-LDH and a certain amount of CuI were added to a glass involving 20 mL alcohol. The mixed solution was stirred continuously for one hour. The composite was obtained after removing ethanol at 80 ℃ and was named CI-n (n = 5, 10, 15, 20). Contents of CoAl-LDH and CuI in the composite are shown in Table 3.

Characterization. X-ray diffraction (XRD: Rigaku RINT-2000, Cu Kα, λ = 0.15418 nm) was employed to reveal the crystal structures of the catalysts the surface morphology of which was shown by scanning electron microscope (SEM: ZEISS EVO 10). Surface element valence state of catalysts was explored by the X-ray photoelectron spectroscopy (XPS: ESCALAB Xi+). The optical performance of catalysts was assessed via the UV-vis DRS (perkinelmerLambda-750, $BaSO_4$ as the reference). Litesizer 500 was used to measure Zeta potentials of CoAl-LDH and CuI. The Brunauer-Emmett-Teller (BET) specific surface area of samples was collected on ASAP 2460. The photoluminescence (PL) spectra and time-resolved photoluminescence (TR-PL) of samples were tested by FluoroMax-4 (HORIBA) and (Fluorohub-B).

Table 3. Amount of CoAl-LDH and CuI

Composites	CuI (g)	CoAl-LDH (g)
CI-5	0.01	0.2
CI-10	0.02	0.2
CI-15	0.03	0.2
CI-20	0.04	0.2

The linear sweep voltammetry (LSV) curves of catalysts were assessed in the workstation (VersaSTAT4-400, AMETEK) containing standard three-electrode cell (counter electrode: platinum electrode; reference electrode: saturated calomel electrode, SCE). The coated with catalysts f-doped tin oxide (FTO) glass (1×1 cm^2) were used as working electrode, and Na_2SO_4 0.5 M aqueous solution as the electrolyte.

The quartz bottle (62 mL) was employed to evaluate the photocatalytic hydrogen evolution performance of materials. Amounts of catalysts and eosin Y (EY) are 0.01 and 0.01 g, respectively. The 15% v/v triethanolamine (TEOA) solution (30 mL) was used as holes consuming reagent, the multi-channel photochemical reaction system (5 W LED white light; PCX50B Discover) as the photocatalytic reaction equipment, and the gas chromatograph (Tianmi GC7900, TCD, 13X columns, N_2 as carrier) was employed to analyze the gas produced. The calculation of the apparent quantum efficiency at different wavelengths is shown in equation (2).

$$\mathrm{AQE}=\frac{2\times\text{the number of evolved hydrogen molecules}}{\text{the number of incident photon}}\times 100\% \qquad (2)$$

ACKNOWLEDGEMENTS

This work was financially supported by the National Natural Science Foundation of China (22062001).

AUTHOR CONTRIBUTIONS

Yue Cao and Hongqian Gou designed the experiments. Zhiliang Jin and Pengfei Zhu contributed reagents, materials and analysis tools. Yue Cao wrote the paper.

AUTHOR INFORMATION

Corresponding author. Email: zl-jin@nun.edu.cn (Z. L. Jin)

COMPETING INTERESTS

The authors declare that they have no competing interests.

ADDITIONAL INFORMATION

Full paper can be accessed via
http://manu30.magtech.com.cn/jghx/EN/10.14102/j.cnki.0254-5861.2022-0042
For submission: https://mc03.manuscriptcentral.com/cjsc

REFERENCES

(1) Yan, T.; Zhang, X, J.; Liu, H.; Jin, Z, L. CeO_2 particles anchored to Ni_2P nanoplate for efficient photocatalytic hydrogen evolution. *Chin. J. Struct. Chem.* **2022**, 41, 2201047-2201053.

(2) Zhang, J. W.; Cheng, C. C.; Xing, F. S.; Chen, C.; Huang, C. J. 0D β-$Ni(OH)_2$ nanoparticles/1D $Mn_{0.3}Cd_{0.7}S$ nanorods with rich S vacancies for improved photocatalytic H_2 production. *Chem. Eng. J.* **2021**, 414, 129157.

(3) Meng, X. Y.; Yang, J. Y.; Xu, S. M.; Zhang, C. C.; Ma, B. C.; Ding, Y. Integrating Mo_2B_x (x = 1, 4) with CdS for efficient photocatalytic hydrogen production. *Chem. Eng. J.* **2021**, 410, 128339.

(4) Yuan, L.; Jiang, S. M.; Li, Z. Z.; Zhu, Y.; Yu, J.; Li, L.; Li, M. Z.; Tang,

S.; Sheng, R. R. Photocatalyzed cascade Meerwein addition/cyclization of N-benzylacrylamides toward azaspirocycles. *Org. Biomol. Chem.* **2018**, 16, 2406-2410.

(5) Zhang, L.; Zhang, J.; Yu, H.; Yu, J. Emerging S-scheme photocatalyst. *Adv. Mater.* **2022**, 34, 2107668.

(6) Tang, S. P.; Fu, Z. H.; Li, Y.; Li, Y. J. Study on boron and fluorine-doped C_3N_4 as a solid activator for cyclohexane oxidation with H_2O_2 catalyzed by 8-quinolinolato iron^{III} complexes under visible light irradiation. *Appl. Catal. A: Gen.* **2020**, 590, 117342.

(7) Zhong, W.; Gao, D. D.; Yu, H. G.; Fan, J. J.; Yu, J. G. Novel amorphous $NiCuS_x$ H_2-evolution cocatalyst: optimizing surface hydrogen desorption for efficient photocatalytic activity. *Chem. Eng. J.* **2021**, 419, 129652.

(8) Chen, P.; Liu, F.; Ding, H. Z.; Chen, S.; Chen, L.; Li, Y. J.; Au, C. T.; Yin, S. F. Porous double-shell CdS@C_3N_4 octahedron derived by in situ supramolecular self-assembly for enhanced photocatalytic activity. *Appl. Catal. B Environ.* **2019**, 252, 33-40.

(9) Tang, N. M.; Li, Y. J.; Chen, F. T.; Han, Z. Y. In situ fabrication of a direct Z-scheme photocatalyst by immobilizing CdS quantum dots in the channels of graphene-hybridized and supported mesoporous titanium nanocrystals for high photocatalytic performance under visible light. *RSC Adv.* **2018**, 8, 42233-42245.

(10) Lin, X.; Du, S. W.; Li, C. H.; Li, G. J.; Li, Y. J.; Chen, F. T.; Fang, P. F. Consciously constructing the robust NiS/g-C_3N_4 hybrids for enhanced photocatalytic hydrogen evolution. *Catal. Lett.* **2020**, 150, 1898-1908.

(11) Wang, P.; Yang, M.; Tang, S. P.; Chen, F. T.; Li, Y. J. Preparation of cellular C_3N_4/$CoSe_2$/GA composite photocatalyst and its CO_2 reduction activity. *Chem. J. Chin. U.* **2021**, 42, 1924-1932.

(12) Jin, Z. L.; Li, Y. B.; Hao, X. Q. Ni, Co-based selenide anchored g-C_3N_4 for boosting photocatalytic hydrogen evolution. *Acta Phys. -Chim. Sin.* **2021**, 37, 1912033.

(13) Pan, J. W.; Guan, Z. J.; Yang, J. J.; Li, Q. Y. Facile fabrication of $ZnIn_2S_4$/SnS_2 3D heterostructure for efficient visible-light photocatalytic reduction of Cr(VI). *Chin. J. Catal.* **2020**, 41, 200-208.

(14) Wang, M.; Zhang, G. X.; Guan, Z. J.; Yang, J. J.; Li, Q. Y. Photocatalytic hydrogen evolution: spatially separating redox centers and photothermal effect synergistically boosting the photocatalytic hydrogen evolution of $ZnIn_2S_4$ nanosheets. *Small* **2021**, 17, 2170074.

(15) Liu, J. F.; Wang, P.; Fan, J. J.; Yu, H. G.; Yu, J. G. In situ synthesis of Mo_2C nanoparticles on graphene nanosheets for enhanced photocatalytic H_2-production activity of TiO_2. *ACS Sustainable Chem. Eng.* **2021**, 9, 3828-3837.

(16) Zhang, J. Y.; Liao, H. G.; Sun, S. G. Construction of 1D/1D WO_3 nanorod/TiO_2 nanobelt hybrid heterostructure for photocatalytic application. *Chin. J. Struct. Chem.* **2020**, 39, 1019-1028.

(17) Geng, J. H.; Zhao, L. L.; Wang, M. M.; Dong, G. H.; Ho, W. K. The photocatalytic NO-removal activity of g-C_3N_4 significantly enhanced by the synergistic effect of Pd^0 nanoparticles and N vacancies. *Environ. Sci.: Nano.* **2022**, 9, 742-750.

(18) Liu, J. L.; Dong, G. H.; Jing, J.; Zhang, S. Y.; Huang, Y.; Ho, W. K. Photocatalytic reactive oxygen species generation activity of TiO_2 improved by the modification of persistent free radicals. *Environ. Sci.: Nano.* **2021**, 8, 3846-3854.

(19) Liu, Y.; Hao, X. Q.; Hu, H. Q.; Jin, Z. L. High efficiency electron transfer realized over NiS_2/$MoSe_2$ S-scheme heterojunction in photocatalytic hydrogen evolution. *Acta Phys. -Chim. Sin.* **2021**, 37, 2008030.

(20) Li, X. B.; Liu, J. Y.; Huang, J. T.; He, C. Z.; Feng, Z. J.; Chen, Z.; Wan, L. Y.; Deng, F. All organic S-scheme heterojunction PDI-Ala/S-C_3N_4 photocatalyst with enhanced photocatalytic performance. *Acta Phys. -Chim. Sin.* **2021**, 37, 2010030.

(21) Jiang, Z. M.; Chen, Q.; Zheng, Q. Q.; Shen, R. C.; Zhang, P.; Li, X. Constructing 1D/2D Schottky-based heterojunctions between $Mn_{0.2}Cd_{0.8}S$ nanorods and Ti_3C_2 nanosheets for boosted photocatalytic H_2 evolution. *Acta Phys. -Chim. Sin.* **2021**, 37, 2010059.

(22) Liu, C.; Mao, S.; Shi, M. X.; Wang, F. Y.; Xia, M. Z.; Chen, Q.; Ju, X. H. Peroxymonosulfate activation through 2D/2D Z-scheme CoAl-LDH/BiOBr photocatalyst under visible light for ciprofloxacin degradation. *J. Hazard. Mater.* **2021**, 420, 126613.

(23) Xia, S. J.; Zhang, G. H.; Gao, Z. Y.; Meng, Y.; Xie, B.; Lu, H. F.; Ni, Z. M. 3D hollow Bi_2O_3@CoAl-LDHs direct Z-scheme heterostructure for visible-light-driven photocatalytic ammonia synthesis. *J. Colloid Interface Sci.* **2021**, 604, 798-809.

(24) Li, H. Y.; Hao, X. Q.; Liu, Y.; Li, Y. B.; Jin, Z. L. $Zn_xCd_{1-x}S$ nanoparticles dispersed on CoAl-layered double hydroxide in 2D heterostructure for enhanced photocatalytic hydrogen evolution. *J. Colloid Interface Sci.* **2020**, 572, 62-73.

(25) Zou, Z.; Wu, L.; Yang, F. Q.; Cao, C. L.; Meng, Q. G.; Luo, J. H.; Zhou, W. Z.; Tong, Z. K.; Chen, J. W.; Chen, S. X.; Zhou, S. D.; Wang, J.; Deng, S. G. Delicate tuning of the Ni/Co ratio in bimetal layered double hydroxides for efficient N_2 electroreduction. *ChemSusChem* **2022**, 15, e202200127.

(26) Wang, Q.; O'Hare, D. Recent advances in the synthesis and application of layered double hydroxide (LDH) nanosheets. *Chem. Rev.* **2012**, 7, 4124-4155.

(27) Sun, M. J.; Hu, J. Y.; Zhai, C. Y.; Zhu, M. S.; Pan, J. G. CuI as hole-transport channel for enhancing photoelectrocatalytic activity by constructing CuI/BiOI heterojunction. *ACS Appl. Mater. Interfaces* **2017**, 9, 13223-13230.

(28) Jin, Z. L.; Zhang, L. J.; Wang, G. R.; Li, Y. B.; Wang, Y. B. Graphdiyne formed S-scheme heterojunction composite for efficient photocatalytic hydrogen evolution over rational design novel CuIGD/g-C_3N_4 composite. *Sustain. Energy Fuels* **2020**, 4, 5088-5101.

(29) Fu, J. W.; Xu, Q. L.; Low, J. X.; Jiang, C. J.; Yu, J. G. Ultrathin 2D/2D WO_3/g-C_3N_4 step-scheme H_2-production photocatalyst. *Appl. Catal. B Environ.* **2019**, 243, 556-565.

(30) Tao, J. N.; Yu, X. H.; Liu, Q. Q.; Liu, G. W.; Tang, H. Internal electric field induced S-scheme heterojunction MoS_2/CoAl-LDH for enhanced photocatalytic hydrogen evolution. *J. Colloid Interface Sci.* **2021**, 585, 470-479.

(31) Xiang, K.; Xu, Z. C.; Qu, T. T.; Tian, Z. F.; Zhang, Y.; Wang, Y. Z.; Xie, M. J.; Guo, X. K.; Ding, W. P.; Guo, X. F. Two dimensional oxygen-vacancy-rich Co_3O_4 nanosheets with excellent supercapacitor performances. *Chem. Commun.* **2017**, 53, 12410-12413.

(32) Wu, Y. L.; Li, Y. J.; Zhang, L. J.; Jin, Z. L. NiAl-LDH in-situ derived Ni_2P and ZnCdS nanoparticles ingeniously constructed S-scheme heterojunction for photocatalytic hydrogen evolution. *ChemCatChem.* **2022**, 14, e202101656.

(33) Han, Z. Y.; Li, Y. J.; Chen, F, T.; Tang, S. P.; Wang, P. Preparation of ZnO/Ag_2O nanofibers by coaxial electrospinning and study of their photocatalytic properties. *Chem. J. Chin. U.* **2020**, 2, 308-316.

(34) Lalitha, K.; Sadanandam, G.; Kumari, V, D.; Subrahmanyam, M.; Sreedhar, B.; Hebalkar, N, Y. Highly stabilized and finely dispersed Cu_2O/TiO_2: a promising visible sensitive photocatalyst for continuous production of hydrogen from glycerol: water mixtures. *J. Phys. Chem. C* **2010**, 114, 22181-22189.

DOI: 10.14102/j.cnki.0254-5861.2022-0042

(35) Zhang, Y. H.; Li, Y. L.; Jiu, B. B.; Gong, F. L.; Chen, J. L.; Fang, S. M.; Zhang, H. L. Highly enhanced photocatalytic H_2 evolution of Cu_2O microcube by coupling with TiO_2 nanoparticles. *Nanotechnology* **2019**, 30, 145401.

(36) Sun, D. F.; Huang, C. C.; Yuan, Y.; Ma, Y. L.; Hao, H.; Li, R. X.; Xu, B. S. Synthesis and photocatalytic activity of BiOBr hierarchical structures constructed by porous nanosheets with exposed (110) facets. *Catal. Today* **2019**, 335, 429-436.

(37) Wang, Y. P.; Hao, X. Q.; Zhang, L. J.; Jin, Z. L.; Zhao, T. S. Amorphous Co_3S_4 nanoparticle-modified tubular g-C_3N_4 forms step-scheme heterojunctions for photocatalytic hydrogen production. *Catal. Sci. Technol.* **2021**, 11, 943.

(38) Li, Y. B.; Wang, G. R.; Wang, Y. B.; Jin, Z. L. Phosphating 2D CoAl-LDH anchored on 3D self-assembled $NiTiO_3$ hollow rod for efficient hydrogen evolution. *Catal. Sci. Technol.* **2020**, 10, 2931-2947.

(39) Yan, T.; Liu, H.; Jin, Z. L. Graphdiyne based ternary GD-CuI-$NiTiO_3$ S-scheme heterjunction photocatalyst for hydrogen evolution. *ACS Appl. Mater. Interfaces* **2021**, 13, 24896-24906.

(40) Dong, H. J.; Zuo, Y.; Song, N.; Hong, S. H.; Xiao, M. Y.; Zhu, D. Q.; Sun, J. X.; Chen, G.; Li, C. M. Bimetallic synergetic regulating effect on electronic structure in cobalt/vanadium co-doped carbon nitride for boosting photocatalytic performance. *Appl. Catal. B Environ.* **2021**, 287, 119954.

(41) Li, C. M.; Wu, H. H.; Zhu, D. Q.; Zhou, T. X.; Yan, M.; Chen, G.; Sun, J. X.; Dai, G.; Ge, F.; Dong, H. J. High-efficient charge separation driven directionally by pyridine rings grafted on carbon nitride edge for boosting photocatalytic hydrogen evolution. *Appl. Catal. B Environ.* **2021**, 297, 120433.

(42) Liu, Z. P.; Wang, K. W.; Li, Y. J.; Yuan, S. S.; Huang, G. Q.; Li, X. T.; Li, N. Activation engineering on metallic 1T-MoS_2 by constructing in-plane heterostructure for efficient hydrogen generation. *Appl. Catal. B Environ.* **2022**, 300, 120696.

(43) Wang, H. L.; Cai, Y.; Zhou, J.; Fang, J.; Yang, Y. Crystallization-mediated amorphous Cu_xO (x = 1, 2)/crystalline CuI p-p type heterojunctions with visible light enhanced and ultraviolet light restrained photocatalytic dye degradation performance. *Appl. Surf. Sci.* **2017**, 402, 31-40.

(44) Jin, Z. L.; Cao, Y. Cube Cu_2O modified CoAL-LDH p-n heterojunction for photocatalytic hydrogen evolution. *Int. J. Energy Res.* **2021**, 45, 19014-19027.

Received: February 27, 2022
Accepted: April 6, 2022
Published: June 20, 2022

DOI: 10.14102/j.cnki.0254-5861.2022-0042